state variables (w, v) are related to the minimal form Eq. (19) through a projection operator Eq. (20)

$$\dot{x}=(\Lambda^T-\underline{a}h^T)x+bu \tag{19}$$

$$y=\left[\frac{1}{a_{n+1}}\right]h^Tx+b_{n+1}u$$

$$x=P_1w+P_2v \tag{20}$$

For example if $n=3$ we have

$$P_1(b)=\begin{bmatrix} b_1(\lambda_3-\lambda_1)(\lambda_2-\lambda_1) & \chi_1(\lambda_3-\lambda_1) & b_1 \\ b_1(\lambda_3-\lambda_1) & b_1+b_2(\lambda_3-\lambda_2) & b_2 \\ b_1 & b_2 & b_3 \end{bmatrix}$$

$$P_2=P_1(-\underline{a}) \tag{21}$$

It is well to note that implicit in any of Lion's[1] identification formulations is a stable observer if the "state variable filters" are selected to have strictly L.H.P. poles. The state variable filters outputs (w, v) can always be related through a projection operator to any minimal form state variables.

It is anticipated that this algorithm will be most successful in a closed loop adaptive control application, where the adaptive control law is computed so as to give some desired fixed closed-loop characteristics. In this case the design parameters are based on the desired fixed closed loop system, and hence may be pre-selected.

V. Practical Considerations

In general the previous identification algorithm is numerically inefficient, that is the required digital integration step size may be extremely small. In this section transformations are presented that result in efficient digital computer implementation of the aforementioned. These transformations are applicable to algorithms of Refs. 7,5,6 and 3. A "numerically well conditioned identifier" is defined next.

If the digital computer integration step size for satisfactory system identification is of the same order as that required for digital computer modeling of the (unknown) system, then the identifier is said to be "well conditioned." The cause of poor numerical conditioning becomes apparent from Eqs. (7,10,and11), that is

$$\dot{v}_1\cong-\dot{v}_1\left[\sum_1^m\delta_1w_1^2+\delta_{n+1}u^2+\sum_2^n\gamma_iv_1^2+\gamma_{n+1}y^2\right]+\cdots \tag{22}$$

The quantity in the brackets is inversely proportional to the integration step size required for the identifier.

The conditioning problem is one of proper signal scaling. Two known scaling parameters applied to the unknown system input and output (u, y) are given by Eq. (23)

$$u'=\Gamma_1u, \qquad y'=\Gamma_1\Gamma_2y \tag{23}$$

where Γ_1 is self explanatory, and Γ_2 is selected so as to match the signal power content of u and y. Finally a collection of scaling parameters (φ_i) are introduced so that the M_i of Eq. (2) now become

$$M_i'=\prod_{j=1}^{n}\varphi_i/(s+\lambda_i), \quad i\neq n+1 \tag{24}$$

The φ_i are selected so as to balance the individual signals (w_i, v_i). The previous scaling parameters have been implemented on several examples, and "well conditioned" identifiers have been developed.

VI. Conclusion

It has been shown that for any general input u, the observer described by Eqs. (7, 8, 10, and 11) will asymptotically yield the states and parameters of an nth order linear time-invariant system (2). This observer does not require auxiliary signals to be fed back into it, and hence is very simple to implement (see Fig. 1).

References

[1]Lion, P.M., "Rapid Identification of Linear and Non-Linear Systems," *AIAA Journal*, Vol. 5, Oct. 1967, pp. 1835-1842.

[2]Bryson, A.E. and Luenberger, D.G., "The Synthesis of Regulator Logic Using State-Variable Concepts," *Proceedings of the IEEE*, Nov. 1970.

[3]Luders, G. and Narendra, K.S., "A New Canonical Form for an Adaptive Observer" *IEEE Transactions on Automatic Control*, Vol. AC-19, April 1974, pp. 117-119.

[4]Chen, C.T.., *Introduction to Linear System Theory*, Holt, Rinehart and Winston, New York, 1970.

[5]Marsik, J., "Quick-Response Adaptive Identification," *Identification in Automatic Control Systems*, IFAC, Pt. 2, Sect. 5.5, Institute of Information Theory and Automation, Czechoslovak Academy of Sciences, Academia, Prague, 1968.

[6]Kushner, H.J., "On the Convergence of Lion's Identification Method with Random Inputs," *IEEE Transactions on Automatic Control*, Vol. AC-15, No. 6, Dec. 1970, pp. 652-654.

[7]Molnar, D.O., "New Form for an Adaptive Observer," *AIAA Journal*, Vol. 13, Feb. 1975, pp. 243-244.

Orbit Determination for Mariner 9 Using Radio and Optical Data

G.H. Born* and S.N. Mohan†
Jet Propulsion Laboratory, Pasadena, Calif.

Introduction

THE orbit phase TV pictures of Mars and its natural satellites taken during the Mariner-Mars 1971 mission have been used in conjunction with Earth-based radio data to improve the accuracy of the spacecraft trajectory estimate over that obtained with radio data only. The optical data used for the study described here consisted of 62 wide and narrow angle photographs of Phobos and Deimos and 162 photographs of select surface features of Mars taken over the first 232 revolutions of the Mariner 9 spacecraft. Mariner 9's TV cameras also photographed the natural satellites against a star background during the approach phase. These pictures formed the basis for a highly successful real time navigation demonstration to predict the encounter parameters of Mariner 9 using combined optical and radio data.[1]

The Mariner 9 optical system is described in Ref. 2, which contains a discussion of results and conclusions of the MM'71 Optical Navigation Demonstration as well as copies of all papers written to date on the optical navigation aspects of the mission. The Mariner 9 trajectory and radio data related

Presented as Paper 74-829 at the AIAA Mechanics and Control of Flight Conference, Anaheim, California, Aug. 5-9, 1974; submitted September 26, 1974; revision received March 17, 1975. This paper presents the results of work carried out at the Jet Propulsion Laboratory, California Institute of Technology under Contract NAS 7-100, sponsored by the National Aeronautics and Space Administration.

Index category: Spacecraft Navigation, Guidance, and Flight Path Control Systems.

*Member of the Technical Staff, Mission Analysis Division. Member AIAA.

†Senior Research Engineer, Mission Analysis Division.

navigation activities during both the approach and orbit phase are described in Ref. 3 and 4. Star images were not available in the orbit phase satellite pictures since the required shutter times would have overexposed satellite images. Consequently, TV pointing information for both the satellite and Mars' landmark pictures was extracted from engineering telemetry data. Engineering data yields pointing accurate to 0.02° (1σ) as opposed to 0.002° (1σ) whenever star images (known inertial directions) are available.

It is well known that Doppler solutions for the state of a spacecraft orbiting a distant body are an order of magnitude less accurate in the node of the orbit relative to the plane of the sky (referred to as Ω_{pos}) than any other component of the state. The plane of the sky is the plane perpendicular to the Earth-Mars direction. The determination of Ω_{pos} depends on relative Earth-Mars motion which is a slowly varying quantity. References 4 and 5 give more detail regarding the indeterminacy of Ω_{pos}. For Mariner 9, the standard deviation in the discontinuities for Ω_{pos} from solutions based on Doppler data ranged from 0.02-0.04° throughout the mission depending on tracking coverage and data noise.[3] Although optical data can be very effective in determining Ω_{pos} when combined with short arcs (less than one orbit) of radio data,[6] the scarcity of optical data taken by Mariner 9 of the satellites and repeatedly observed Mars surface features precluded a short arc demonstration with real data. However, a long arc analysis of combined optical and radiometric data from Mariner 9 was performed.

Method of Solution

The radio plus satellite imaging data were processed independently of the radio plus Mars imaging data. While the processing of the data types was similar, there were some procedural differences as outlined in the next two sections.

Radio Plus Satellite Imaging Data

The radio and satellite imaging data were processed in a two-stage filter. The first stage of the filter was a conventional batch processor used to fit short arcs of Doppler data to determine an apoapsis state vector for each orbit.[7] These state vectors, referred to as normal points, were used as observables for the second stage of the filter. Here they were processed simultaneously with the coordinates for the center of mass (assumed to be at the center of the figure) of the satellites to yield solutions for both the state of the satellites and the spacecraft. Coordinates of the center of figure of the satellites were obtained by using high fidelity prints of the TV photographs together with computer generated overlays which modeled the satellite as a triaxial ellipsoid and accounted for the solar phase angle.

A first-order analytical theory which includes the effects of zonal and tesseral harmonics as well as solar gravity and radiation pressure, was used to propagate the motion of Mariner 9, Phobos, and Deimos in the second stage of the filter. Since Mariner 9 was in shallow resonance with Mars' even-order tesseral harmonics, large downtrack perturbations (1000 km) were induced in the orbital motion.[3] As a result, a first-order analytical theory was inadequate to model the spacecraft's motion; consequently, the theory was extended to include the dominant second-order effects of resonance.[8] Use of analytical theories allows rapid and inexpensive processing of the data; because of this, processing of long arcs of data is feasible.

Radio Plus Mars Surface Imaging Data

The process of physically reducing the information from landmark photographs to a computationally amenable form and the steps involved in data processing are described in Ref. 9. A brief outline of the method of solution consists of: a) generation of prefit data residuals based on the celestial attitude of the imaging instrument estimated from engineering telemetry data and the estimated spacecraft state from Doppler observations; b) generation of a time history of orbital elements of the Doppler-determined orbits in the Earth's plane-of-sky coordinates (instantaneous), after deleting known effects of geometry (from the moving plane-of-sky) and secular dynamic effects contributed by the second-degree zonal harmonic, J_2; c) the time history determined from Doppler tracking of the node of the orbit in the moving plane-of-sky has discontinuities.[3] The actual node can be compared with an apriori continuous mode, thus ascribing an a priori Δ node (designated $\Delta\Omega_{pos}$) corresponding to each orbit; d) use the prefit data residuals generated in step 1 to determine a constant correction to the apriori continuous node. The resulting solution for Ω_{pos} can then be compared with the a priori radio mean, as well as the best estimate resulting from observations of the natural satellites.

A sequential filter algorithm was used for processing both the satellite and Mars imaging data. A sequential filter was chosen since it facilitated modeling certain TV bias parameters as Gauss Markov processes and allowed estimation of TV pointing direction.

Comparison of Ω_{pos} History for Radio and Optical Data

The results for the radio and the combined radio plus imaging data are shown in Fig. 1. The ordinate is the change in Ω_{pos} from a reference value obtained from one of the preliminary radio plus satellite data solutions. The abscissa is the probe ephemeris segment number which refers to the 21 segments of Doppler-determined orbits obtained from the Mariner 9 navigation team. The 21 associated values of Ω_{pos} obtained from the Doppler solutions are shown as solid lines for each probe ephemeris segment. The mean values of these "radio only" solutions before and after the second orbital trim maneuver are also shown on this plot as well as the values obtained from the various radio plus imaging data solutions.

The solution labeled "radio + Phobos/Deimos" was obtained by solving simultaneously for the state of the spacecraft and the satellites, the spin axis direction of Mars and TV parameters. The optical data were weighted at 0.02°. The radio normal points were weighted in a manner to be consistent with the accuracy of the analytical theory and the accuracy of Ω_{pos} from the Doppler solutions. The values used were $\sigma_{I_{pos}} = \sigma_{\omega_{pos}} = 0.005°$ and $\sigma_{\Omega_{pos}} = 0.05°$. The values of *a*, *e*, and *M* were fixed to the Doppler determined values since the optical data was too inaccurate to improve these quantities. Note that the data weight essentially constrains the orientation of the orbit, except for Ω_{pos}, to that of the radio normal points. The formal uncertainty on Ω_{pos} from the combined radio and satellite data solution is $\sigma_{\Omega_{pos}} = 0.004°$. If only the satellite data is processed, essentially the same solution for Ω_{pos} is obtained; however, $\sigma_{\Omega_{pos}} = 0.014°$. This uncertainty should be representative of the actual estimation error since it is compatible with the differences between the

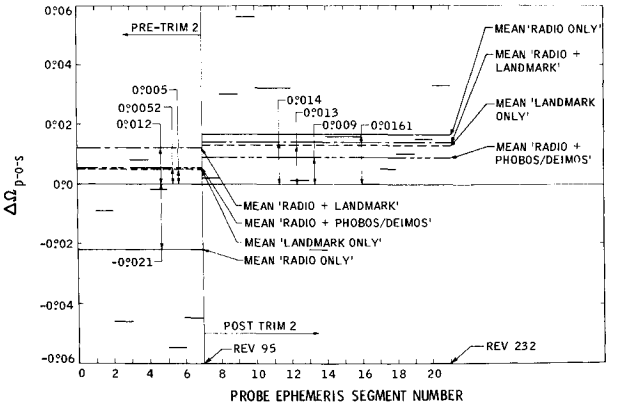

Fig. 1 Ω_{pos} solutions for radio and radio plus imaging data.

Table 1 Results for radio optical data

	Pre-Trim II[a] mean $\Delta\Omega_{pos}$, deg	Post-Trim II mean $\Delta\Omega_{pos}$, deg
1. A priori "radio only" mean	−0.021	+0.016
2. Landmark only	+0.005	+0.013
3. Radio + landmark	+0.012	+0.014
4. Radio + Phobos/Deimos	+0.005	+0.009
2-4	+0.000	+0.004
3-4	+0.007	+0.005

[a]Trim II occurred in the 95th satellite orbit.

value of Ω_{pos} obtained from the satellite and Mars imaging data.

The solution for the landmark data were obtained based on the following assumptions: a) It is assumed that the radio mean Ω_{pos} differs from the "true" mean Ω_{pos} (to be determined) by a constant value contained in the 1σ dispersion of the Doppler determined node values. In other words, it is assumed that the absolute Ω_{pos}, as determined from Doppler observations, has a mean value whose uncertainty is limited to 0.05° (1σ). Under this assumption, the result obtained after addition of Mars imaging data is referred to as the "radio and landmark" solution.

b) In this case, it is assumed that although the disperson in $\Delta\Omega_{pos}$ is contained in a band of ±0.05° the "true" mean is unknown (i.e., a priori $\sigma_{\Omega pos} \to \infty$). The solution resulting from addition of imaging data is therefore labeled as the "landmark only" solution. The purpose of including the variations is to determine the consistency of results under both hypotheses. Results for all data types are summarized in Table 1.

The results show close agreement between the landmark only, radio + landmark, and radio + Phobos/Deimos solutions. The mean Ω_{pos} values from 2, 3, and 4 listed in the table have a mutual disagreement contained with +0.007/−0.000°. Consequently, it has been shown that observations of natural satellites and of the planetary surface independently yield consistent solutions of the mean Ω_{pos}, thereby demonstrating the effectiveness of imaging data in improving radiometric accuracies.

Conclusions

An analysis has been made of post-flight orbit determination capabilities for the Mars orbit phase of the Mariner-Mars 1971 mission using Doppler data combined with optical data in the form of TV photographs of the natural satellites and Mars' surface features. It has been shown that the combined data yield a solution which is a factor of 3-5 better than that obtained from Doppler only solutions for the node of the orbit relative to the plane perpendicular to the Earth-Mars line. Consequently, these optical data types have a demonstrated potential to significantly improve planetary orbiter navigation accuracies.

References

[1]Duxbury, T.C., Born, G.H., and Jerath, N., "Viewing Phobos and Deimos for Navigating Mariner 9," *Journal of Spacecraft and Rockets*, Vol. 11, April 1974, pp. 215-222.

[2]Born, G.H., Duxbury, T.C., Breckenridge, W.G., Acton, C.H., Mohan, S., and Ohtakay, H., "Mariner Mars 1971 Optical Navigation Demonstration Final Report," Rept. TM 33-683, April 1974, Jet Propulsion Lab., Pasadena, Calif.

[3]Born, G., Christensen, E., Ferrari, A., Jordan, J., and Reinbold, S., "The Determination of the Satellite Orbit of Mariner 9," *Celestial Mechanics*, Vol. 9, May 1974, pp. 395-414.

[4]O'Neil, W.J., Jordan, J. F., Zielenbach, J. W., Mitchell, R. T., Webb, W. A., and Koskela, P. E., "Satellite Orbit Determination Section," Rept. TR-32-1586, Nov. 1973, *Mariner 9 Navigation*, Jet Propulsion Lab., Pasadena, Calif.

[5]Lorell, J., "Orbit Determination of a Lunar Satellite," *The Journal of the Astronautical Sciences*, Vol. XI, Spring 1964, pp. 1-7.

[6]Duxbury, T. and Born, G.H., "Tracking Phobos and Deimos Aboard an Orbiting Spacecraft," Paper 71-372, Ft. Lauderdale, Fla., Aug. 1971.

[7]Ferrari, A.J. and Christensen, E.J., "Mars Gravity Derived from the Long-Period Motion of Mariner 9," AAS/AIAA Astrodynamics Conference, Vail, Colo., July 1973.

[8]Born, G.H., "Mars Physical Parameters as Determined from Mariner 9 Observations of the Natural Satellites and Doppler Tracking," *Journal of Geophysical Research*, Vol. 79, Nov. 1974, pp. 4837-4844.

[9]Mohan, S.N., "Pole Direction, Cartography and the Shape of Mars," presented at the International Association of Planetology Symposium of the 24th International Geological Congress, Montreal, Canada, Aug. 1972.

Prototype North-South Stationkeeping Ion Thruster

W. D. Ramsey* and E. L. James*
Xerox Electro-Optical Systems, Pasadena, Calif.

Introduction

FOR north-south stationkeeping missions on synchronous communication satellites a 17 mN MESC cesium ion thruster has been developed. Thruster specifications and operating parameters were chosen for compatibility with a spacecraft power system incorporating an efficient, lightweight energy storage device such as a nickel-hydrogen battery. In operation, the battery would be slowly charged for approximately 20 hr/day, then discharged at the multi-hundred watt level for several hours to power the stationkeeping thruster system. The advantages of this approach are high-thruster efficiency in the multi-mN thrust range, high-thrusting efficiency (since all operation occurs near orbit node crossings), and short total operating time (which facilitates ground testing and qualification).

Thruster Design

The thruster is designed around a 14 cm diam discharge chamber which produces a 12-cm-diam ion beam. A schematic diagram is shown in Fig. 1. The discharge chamber is spun from soft iron into a grooved hemisphere. Placovar (Pt77 Co23) ring magnets fit into the grooves and are magnetized normal to the discharge chamber surface. The MESC geometry[1] is completed by annular boundary anodes spaced between the magnets. A preheater is attached to the discharge chamber and is used to reduce condensation of cesium on the chamber walls and electrodes during startup.

Five percent of the cesium propellant is introduced into the main discharge through the hollow cathode. The remaining 95% of the cesium propellant is introduced through a bypass feed ring which operates at anode potential to prevent power loss due to ion bombardment. No plasma anode, striker, baffle, or keeper are required in this design. The ion beam is extracted by a pair of dished electrodes. Aperture location is compensated for differential thermal expansion between the accelerator and screen and for electrode curvature. That is, at

Presented as Paper 74-1119 at the AIAA/SAE 10th Propulsion Conference, San Diego, Calif., October 21-23, 1974; submitted November 18, 1974; revision received April 10, 1975. This paper is based in part upon work performed under the sponsorship of the International Telecommunications Satellite Organization (INTELSAT). Any views expressed herein are not necessarily those of INTELSAT.

Index category: Electric and Advanced Space Propulsion.

*Physicist, Instrumentation and Propulsion Department.